Observation of Core Phase ScS from the M_w 9.0 Tohoku-Oki Earthquake with High-Rate GPS

by Aizhi Guo, Yong Wang, Zhiwei Li, Sidao Ni, Wenbo Wu, Genyou Liu, Yong Zheng, and Mark Simons

Online Material: Supplemental figures.

INTRODUCTION

High-rate Global Positioning Systems (GPS) observations can record ground motions from moderate to strong earthquakes at distances of a few kilometers up to thousands of kilometers (Larson *et al.*, 2003; Bock *et al.*, 2004; Ohta *et al.*, 2006; Wang *et al.*, 2007; Davis and Smalley, 2009; Delouis *et al.*, 2010; Shi *et al.*, 2010; Yue and Lay, 2011). These observations detect strong signals such as *S* wave and surface waves (Kouba, 2003; Larson *et al.*, 2003; Irwan *et al.*, 2004; Ohta *et al.*, 2006; Wang *et al.*, 2007; Davis and Smalley, 2009; Shi *et al.*, 2010), as well as relatively weaker seismic phases such as *P* waves (Avallone *et al.*, 2011). Seismic phases arriving later than surface waves have been rarely reported. Although it has been confirmed that arbitrarily large seismic signals are recorded with high-rate GPS (Bock *et al.*, 2004), we assess here the lower limit of signals from earthquakes that can be recovered from high-rate GPS records.

Benefits of exploiting high-rate GPS in earthquake source studies include the ability to detect arbitrarily large dynamic ground motions that do not clip in the presence of strong ground motion and accurate recording of ground displacements without needing to doubly integrate acceleration records of strong-motion seismometers (Graizer, 2010). As a result, high-rate GPS records are now routinely used in studies of earthquake source parameters and rupture process independently of, or jointly with, seismological observations (Miyazaki *et al.*, 2003; Ji *et al.*, 2004; Bilich *et al.*, 2008; Yokota *et al.*, 2009; Avallone *et al.*, 2011; Yue and Lay, 2011; Bock *et al.*, 2011; Crowell *et al.*, 2012). Though whole waveforms of high-rate GPS records have been employed in modeling earthquake source processes, it is not certain whether the wiggles following surface waves are true ground-motion signals or contamination from GPS signal propagation effects such as multipath or ionospheric distortion. Accordingly, very few phases following the arrival time of surface waves have been confirmed on high-rate GPS records, primarily because of the inherently lower signal-to-noise ratio (SNR). Identification and retrieval of the weaker secondary arrivals from high-rate GPS records would further confirm capability of GPS in recording ground motions, and thus lead to improved broadband seismograms via collated GPS and seismometers (Bock *et al.*, 2011). Among the later arrivals, the seismic phase *ScS* is expected to be strong due to the complete reflection at the core–mantle boundary between the solid mantle and the liquid outer core where shear waves disappear. Moreover, *ScS* is far behind surface waves at close distances (less than 20°) where contamination of the surface-wave coda is weak.

Here, we present a record section of seismograms retrieved from high-rate GPS from the 2011 Tohoku earthquake wherein we observe a weak but coherent seismic phase that we associate with *ScS*. This inference is supported by comparison of the high-rate GPS records with seismic records and synthetic seismograms.

THE 2011 TOHOKU-OKI EARTHQUAKE

The great 11 March 2011 M_w 9.0 Tohoku-Oki earthquake (5.31×10^{29} dyn·cm; Global Centroid Moment Tensor [CMT] http://earthquake.usgs.gov/earthquakes/eqinthenews/2011/usc0001xgp/neic_c0001xgp_gcmt.php, last accessed 23 April 2013) is one of the largest earthquakes instrumentally recorded (Ammon *et al.*, 2011; Simons *et al.*, 2011; Fig. 1). The mainshock of the Tohoku earthquake ruptured an area about 200 × 200 km in extent with a maximum slip of 60 m (Simons *et al.*, 2011; Yue and Lay, 2011). The CMT solution indicates a faulting mechanism of mostly thrust slip, consistent with the northeast subduction of the Pacific plate.

HIGH-RATE GPS DATA AND PROCESSING METHOD

We collected 1-Hz high-rate GPS data from 192 stations in the Crustal Movement Observation Network of China (CMONOC) spanning the period of the earthquake (Fig. 1). Each of the CMONOC GPS stations is equipped with a Trimble NetR8 GPS receiver and choke-ring antenna as well as temperature and pressure sensors. Epicentral distances of the GPS stations span 1200–5500 km from the Tohoku-Oki earthquake.

To process the GPS data, we adopt a Precise Point Positioning (PPP) strategy, which does not require reference

doi: 10.1785/0220120143

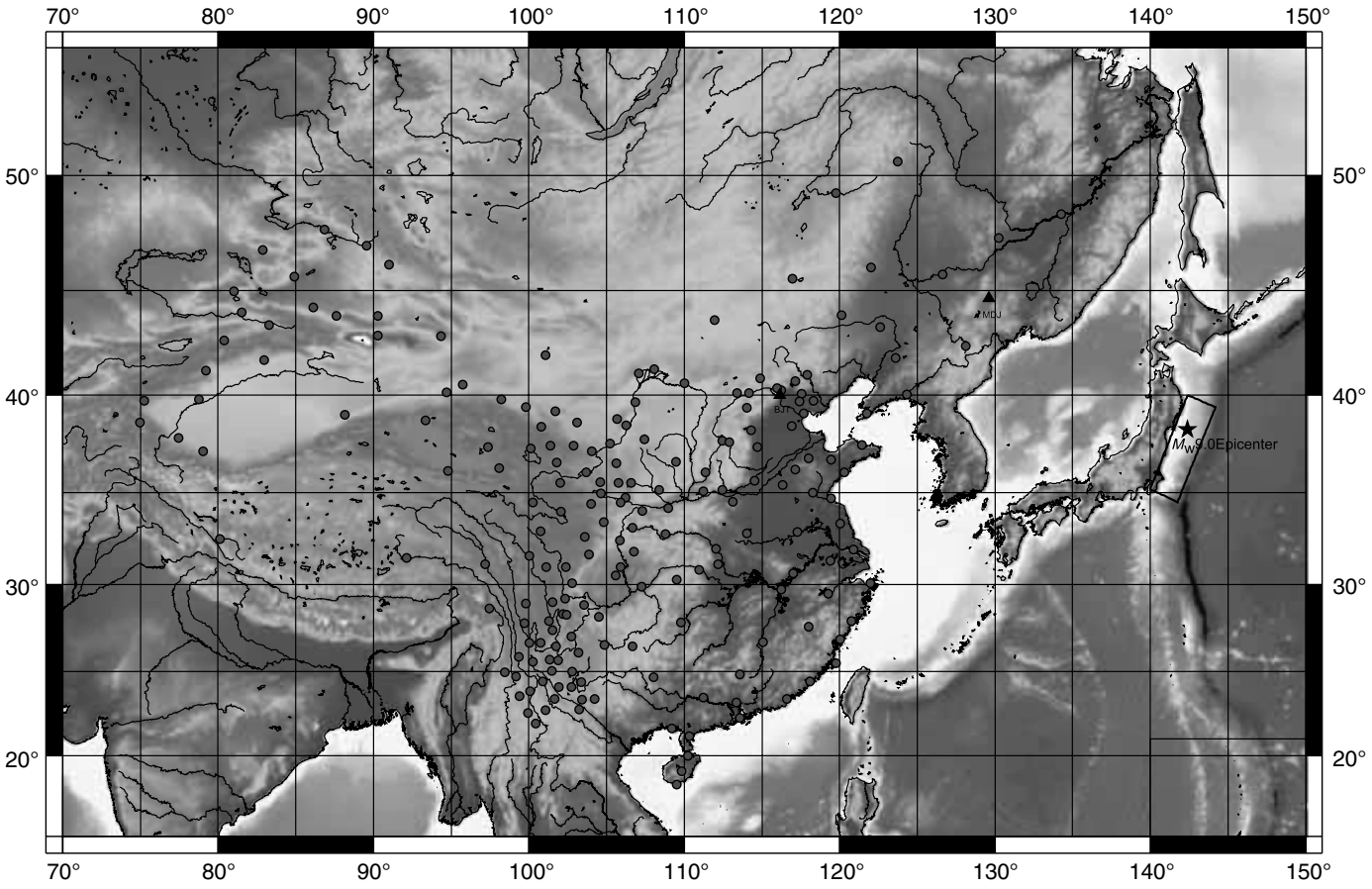

▲ **Figure 1.** Star, the M_w 9.0 Tohoku-Oki earthquake; circles, high-rate GPS stations; and triangles, very broadband seismic stations in China.

stations. Here, we use the software package GPS Inferred Positioning System version 6.0 (GIPSY) developed by the Jet Propulsion Laboratory (JPL; Blewitt, 1989; Zumberge *et al.*, 1997; Bertiger *et al.*, 2010). The GIPSY software resolves ambiguities of an individual station with the help of wide-lane and phase-bias estimation that is calculated from the global GPS network (Bertiger *et al.*, 2010), thereby achieving high-precision kinematic displacements. JPL's final products (30-s precise clock, 15-minute orbit, wide-lane, and phase-bias products) are fixed when estimating receiver clocks, random-walk zenith troposphere delay (5×10^{-8} km $s^{1/2}$) and receiver position (in white-noise mode) as well as integer-cycle ambiguities.

The kinematic-displacement time series are still affected by multipath errors, which are related to satellite-receiver geometry and environments around GPS antennas. We mitigate multipath errors in the high-rate GPS displacement time series by applying Aspect Repeat Time Adjustment (ARTA). We use two extra days of data (DOY 68–69, 2011) for each station following methods by Larson *et al.* (2007).

IDENTIFICATION OF THE CORE PHASE *ScS*

We processed 1-Hz GPS for a 2000 s time window following the initiation time of the earthquake to obtain three-component ground-displacement time series for 192 stations. The east–west and north–south components are rotated to radial and tangential directions, thereby facilitating seismic analysis. As the Tohoku-Oki earthquake is mostly a dip-slip event and most stations in China are perpendicular to the strike of the earthquake, the *SH* (tangential components) waves are close to nodal plane (zero amplitude) and radial components are near maximum as expected from their very different radiation pattern. Therefore, the radial components are much stronger (Fig. 2a).

Rayleigh waves are the strongest seismic phase on the record section with an apparent velocity of about 3.8 km/s, as predicted for Rayleigh wave dispersion around 50 s using a continental mantle model. The Rayleigh wave has amplitude around 18 cm (at an epicentral distance of 10°) for stations in northeastern China, and more than 4 cm (at distances of 52°) for stations in the northwestern-most part of China. *S* waves are coherent and strong for all the distances, but with much shorter duration as compared with the Rayleigh wave, consistent with the nature of body waves. *P* waves are clear for distances up to 30°, but their onsets are much weaker for a distance range of 30°–52°. At this range, a long-period signal is observed between *P* and *S*, corresponding to the *W* phase, which is best observed with very broadband seismometers (Kanamori, 1993). The clear observation of the *W* phase in

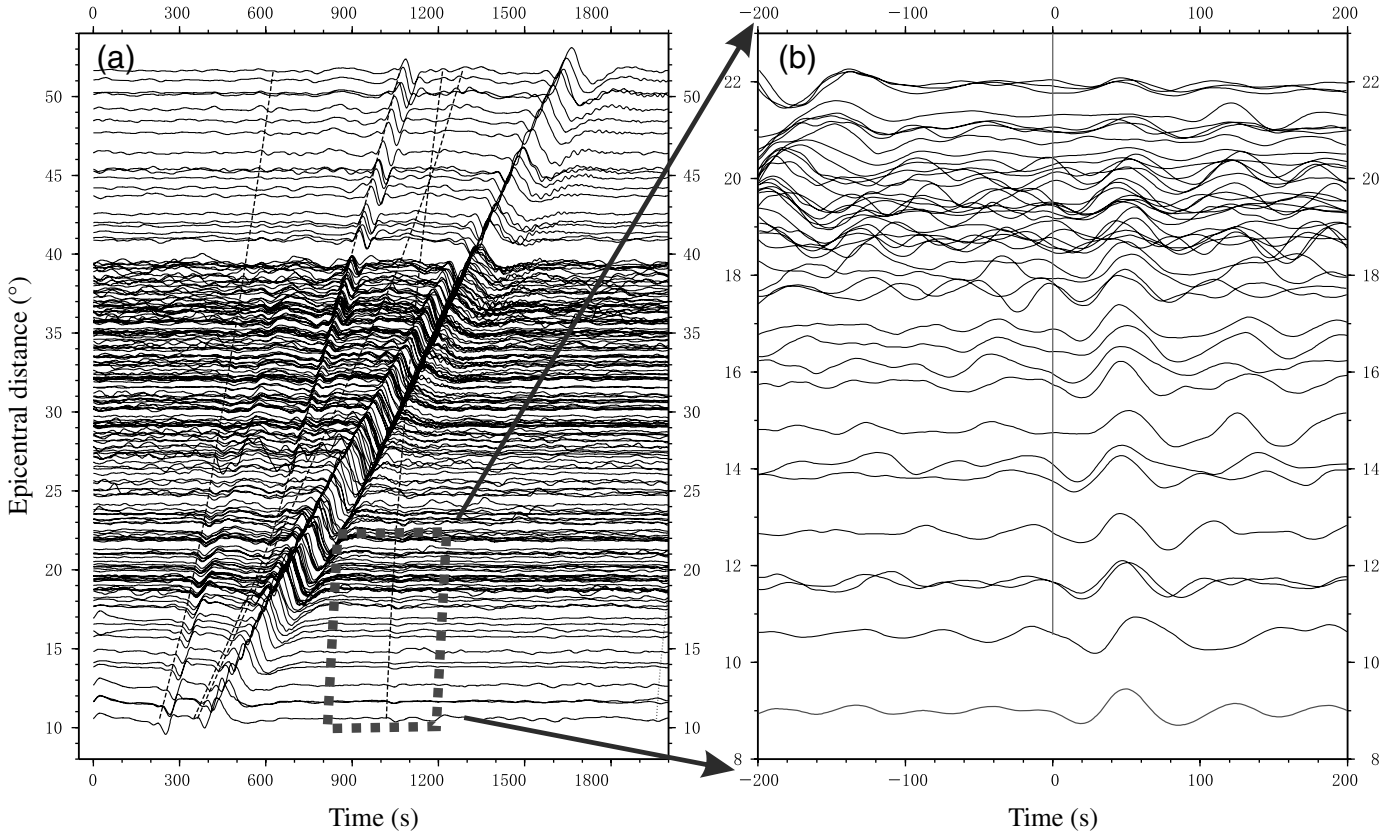

▲ **Figure 2.** (a) Record section (radial component) of 1-Hz GPS displacement for time window from 0 to 2000 s after the earthquake. Dashed lines, indicate theoretical arrival times of *P*, *S*, *R* (Rayleigh), and *ScS*. (b) Zoomed-in record section (radial component) aligned on *ScS* theoretical travel times; gray, stacked *ScS* are displayed in gray.

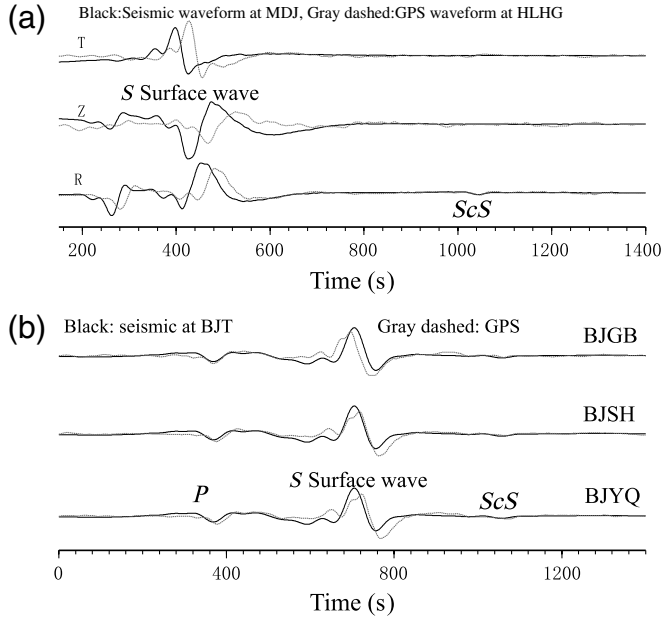

▲ **Figure 3.** (a) Comparison of three-component ground displacement reconstructed from high-rate GPS station HLHG and from seismic station MDJ. Comparison of radial component of ground displacement at (b) dashed in gray, three high-rate GPS stations (BJGB, BJSH, BJYQ), and in black, seismic station BJT.

the high-rate GPS record section suggests that it can be also be exploited for rapid source characterization (Kanamori and Rivera, 2008; Duputel *et al.*, 2011).

For distances of 10° to 22°, there is weak but coherent phase with arrival around 1000 s (Fig. 2a). Its arrival is consistent with the travel time of *ScS* as computed with ray theory for the Preliminary Reference Earth Model (PREM). After the seismograms are aligned on *ScS* theoretical travel times (Fig. 2b), the phase does not show time moveout with distances suggesting that it is probably *ScS*. Stacking after *ScS* travel-time correction for the seismic phase also shows a strong signal with similar wave shape, again arguing for its coherence.

The SNR of the *ScS* phase is not high on high-rate GPS records, in contrast to the clear signal of *P*, *S*, and surface waves (Fig. 3a). For station HLHG in northeastern China, the amplitude of *ScS* is about 6.2 mm and is a little bit above the 4–5 mm resolution of horizontal displacement resolved from high-rate GPS without stacking (Larson *et al.*, 2007). Though clipped at strong ground motion, broadband seismometers are sensitive for small ground displacements. Therefore we compare the high-rate GPS records with seismological records from very broadband seismometers of MDJ and BJT in the IC network of the Incorporated Research Institutions for Seismology (IRIS). We compare the record for GPS station HLHG and seismograph station MDJ. The *P*, *S*, and surface waves on both

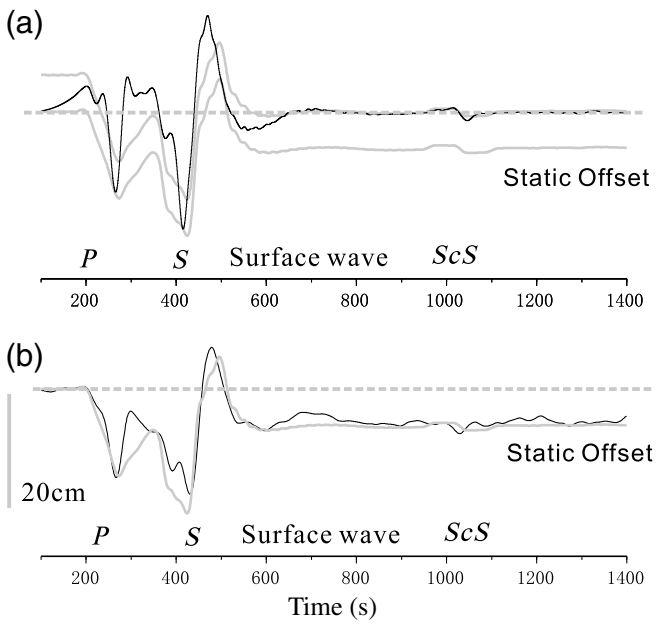

▲ **Figure 4.** (a) Solid black, observed and thick gray, synthetic radial component ground displacement recorded at seismic station MDJ. The seismic recording does not feature a 2.5 cm permanent static offset due to limited bandwidth of seismometers. Upper gray trace, the synthetic waveform shifted by 2.5 cm to fit the seismic ground displacements; lower gray trace, the synthetic waveform computed with mode summation, showing *P*, *S*, surface waveforms, and *ScS*, as well as static offset. (b) Radial component of ground displacement from high-rate GPS station HLHG (black solid line) and synthetic waveform (thick gray line). The GPS record shows permanent static offset, predicted with synthetic seismograms. *ScS* from the GPS record is noisy, but can be resolved with stacking method (Fig. 2b).

records show similar amplitudes, but with obvious timing offsets which can be explained with their difference in epicentral distances and relative small apparent velocity of crustal and mantle phases (3–10 km/s). In contrast, *ScS* has very high apparent velocity at short distances (60 km/s around distance of 10°). Indeed the *ScS* on GPS records and seismograph records arrive almost at the same time despite the 100 km difference in epicentral distances. *ScS* on three GPS (BJGB, BJSH, and BJYQ) records also matches *ScS* on seismograms at BJT well, arguing that *ScS* is observable up to 20°. We emphasize that the very high apparent velocity of *ScS* at short distances requires the PPP mode of high-rate GPS processing for successful observation of *ScS*. Otherwise, even if the reference station is 300 km away for an epicentral distance of 10°, the travel-time difference is only about 5 s, which would be too small as compared with the long rupture time of megathrust earthquakes (> 100 s). In this case, the *ScS* signal retrieved from the reference model would be very weak.

Major phases such as *S* waves from strong aftershocks might be mistaken as secondary phases of the mainshock, but this can be excluded as the source for the observed *ScS* because of their different slowness. In order to further confirm that the coherent phases observed at different GPS stations are true *ScS* from the Tohoku-Oki earthquake, we compare the observation of *ScS* with synthetic seismograms. There have been various methods for computing synthetic seismograms, including purely numerical methods (e.g., Komatitsch and Tromp, 2002a,b; Zhang and Chen, 2006), frequency–wavenumber (*f*-*k*) spectral methods (e.g., Zhu and Rivera, 2002) and normal mode summation (e.g., Dahlen and Tromp, 1998). Among these methods, normal mode summation method takes into account the self-gravity of the Earth, includes all the free oscillation modes of the Earth, and generates full waveforms for a layered spherical or elliptical Earth. It is particularly accurate for long-period synthetic seismograms. Static (permanent) displacements are also accounted for in the normal mode approach. Therefore, we adopt the normal modes to calculate the synthetic seismogram. Source parameters are taken from point-source solution for the Tohoku-Oki earthquake from Global CMT, and source–time function is assumed to be triangular with half duration of 70 s. Figure 4a shows the radial component of the long-period seismic record (black line) observed at MDJ station and the synthetic seismogram (gray bold line). We observe strong major phases such as *P*, *S*, and surface waves as well as *ScS*, which is the strongest phase behind the surface wave. The amplitudes and arrival of the synthetics match well the observed seismometer records both for the major phases and *ScS*. However, due to their limited bandwidth, the seismometers do not record static ground displacement, which is up to 2.5 cm at MDJ station as predicted by the synthetic seismograms. Additionally, there are obvious detailed misfits between the observed and synthetic *ScS* probably due to our overly simple point-source assumption based on the Global CMT. In contrast to direct *P* and *S*, which are widely used in finite-fault inversions, *ScS* has very small ray parameter and can provide extra constraints on source processes of the earthquake. Figure 4b displays the synthetic seismograms (gray bold line) and the displacement observed by high-rate GPS at HLHG. Though there is some noise in the GPS observation, *ScS* can be observed both on the observation and synthetics.

SUMMARY

We collected high-rate GPS data (1-Hz) from 192 stations in China recording the Tohoku-Oki earthquake. Not only do we retrieve *P*, *S*, and surface waves, but we also retrieve the outer-core-reflected *ScS* wave. This inference is supported by comparison with both seismographic records and the synthetic waveforms. However, it is still challenging to include *ScS* waveforms for earthquake source studies, because the complexity of lowermost mantle structure (such as the sharp boundaries and ultra-low velocity zones [ULVZs]) may substantially change amplitude and even waveforms of *ScS* (Helmberger *et al.*, 2000; Ni and Helmberger, 2001; Ni *et al.*, 2002).

For observation of seismic phases with large apparent velocity such as *ScS*, the PPP processing approach is preferred over the double-difference approach. For example, the travel-time difference of *ScS* at distances of 10° and 20° are only

about 25 s, the minor difference in travel time makes *ScS* (duration about 100 s) from the Tohoku-Oki earthquake difficult to observe with the double-difference approach even with a reference station as far as 1000 km away. To demonstrate the distortion of *ScS* due to the double-difference approach, we show *ScS* signals on the east–west component at stations HIA and MDJ and the difference of *ScS* between HIA and MDJ (see Ⓔ supplementary Figs. S1 and S2, available in the electronic supplement that accompanies this paper). The *ScS* signals on HIA and MDJ are similar, but the differenced *ScS* signals are substantially different from *ScS* signals on individual stations (see Ⓔ supplementary Fig. S2 in supplement).

However, signals retrieved with the PPP approach could be contaminated by common mode error (CME), which may be present for multiple reasons (Dong *et al.*, 2006). CME for time scale of days has been explored, but CME from high-rate GPS for a time scale of one hundred to one thousand seconds are little studied. To assess effects of CME on our study, we perform principal component analysis on the high-rate GPS time series from time of 2000–4000 s before the Tohoku-Oki earthquake. On the north–south and east–west components, CME from the first principal component for the time scale of a few thousand seconds has amplitude of less than 3 mm (see Ⓔ Supplemental Fig. S3 in the supplement). But for the up–down direction, CME shows long-period drift and reaches almost 1 cm. For the time scale of 100 s, CME has amplitude of less than 2–3 mm, substantially smaller than the 7 mm displacement observed for *ScS*. Of course, *ScS* signal could be enhanced if the sources of CME are better understood and more advanced processing techniques are available for suppressing CME.

By applying the methods usually used in seismology to high-rate GPS such as stacking and other array analysis techniques, more seismic phases could be identified and retrieved for strong earthquakes. Combined with conventional seismic instrumentation, we should routinely use these plentiful data sources for seismological studies (Bock *et al.*, 2011; Crowell *et al.*, 2012).

ACKNOWLEDGMENTS

This research is supported by National Natural Science Foundation of China (Grant Numbers: 41021003, 40974013, 40974044, and 41074051), and Chinese Academy of Sciences International Partnership Program for Creative Research Teams (CAS/SAFEA) Grant Number KZZD-EW-TZ-05. We would like to thank China's National Earthquake Infrastructure Service for supplying the 1-Hz high-rate GPS data of CMONOC used in our study and JPL for the GIPSY software.

REFERENCES

Ammon, C. J., T. Lay, H. Kanamori, and M. Cleveland (2011). A rupture model of the 2011 off the Pacific coast of Tohoku earthquake, *Earth Planet Space* **63,** no. 7, 693–696, doi: 10.5047/eps.2011.05.015.

Avallone, A., M. Marzario, A. Cirella, A. Piatanesi, A. Rovelli, C. Di Alessandro, E. D'Anastasio, N. D'Agostino, R. Giuliani, and M. Mattone (2011). Very high rate (10 Hz) GPS seismology for moderate-magnitude earthquakes: The case of the M_w 6.3 L'Aquila (central Italy) event, *J. Geophys. Res.* **116,** B02305, doi: 10.1029/2010JB007834.

Bertiger, W., S. Desai, B. Haines, N. Harvey, A. Moore, S. Owen, and J. Weiss (2010). Single receiver phase ambiguity resolution with GPS data, *J. Geodes.* **84,** no. 5, 327–337, doi: 10.1007/s00190-010-0371-9.

Bilich, A., J. Cassidy, and K. M. Larson (2008). GPS seismology: Application to the 2002 $M_w = 7.9$ Denali fault earthquake, *Bull. Seismol. Soc. Am.* **98,** no. 2, 593–606, doi: 10.1785/0120070096.

Blewitt, G. (1989). Carrier phase ambiguity resolution for the Global Positioning System applied to geodetic baselines up to 2000 km, *J. Geophys. Res.* **94,** no. B8, 10,187–10,283, doi: 10.1029/JB094iB08p10187.

Bock, Y., D. Melgar, and B. W. Crowell (2011). Real-time strong-motion broadband displacements from collocated GPS and accelerometers, *Bull. Seismol. Soc. Am.* **101,** no. 6, 2904–2925, doi: 10.1785/0120110007.

Bock, Y., L. Prawirodirdjo, and T. I. Melbourne (2004). Detection of arbitrarily large dynamic ground motions with a dense high-rate GPS network, *Geophys. Res. Lett.* **31,** L06604, doi: 10.1029/2003GL019150.

Crowell, B. W., Y. Bock, and D. Melgar (2012). Real-time inversion of GPS data for finite fault modeling and rapid hazard assessment, *Geophys. Res. Lett.* **39,** L09305, doi: 10.1029/2012GL051318.

Dahlen, F. A., and J. Tromp (1998). *Theoretical Global Seismology*, Princeton University Press, Princeton, 366–376.

Davis, J. P., and R. Smalley Jr. (2009). Love wave dispersion in central North America determined using absolute displacement seismograms from high-rate GPS, *J. Geophys. Res.* **114,** B11303, doi: 10.1029/2009JB006288.

Delouis, B., J.-M. Nocquet, and M. Vallée (2010). Slip distribution of the February 27, 2010 $M_w = 8.8$ Maule Earthquake, central Chile, from static and high-rate GPS, InSAR, and broadband teleseismic data, *Geophys. Res. Lett.* **37,** L17305, doi: 10.1029/2010GL043899.

Dong, D., P. Fang, F. Bock, F. Webb, L. Prawirondirdjo, S. Kedar, and P. Jamason (2006). Spatiotemporal filtering using principal component analysis and Karhunen-Loeve expansion approaches for regional GPS network analysis, *J. Geophys. Res.* **111,** B03405, doi: 10.1029/2005JB003806.

Duputel, Z., L. Rivera, H. Kanamori, G. P. Hayes, B. Hirshorn, and S. Weinstein (2011). Real-time W phase inversion during the 2011 off the Pacific coast of Tohoku earthquake, *Earth Planet Space* **63,** 535–539.

Graizer, V. (2010). Strong motion recordings and residual displacements: What are we actually recording in strong motion seismology? *Seismol. Res. Lett.* **81,** no. 4, 635–639.

Helmberger, D., S. D. Ni, L. X. Wen, and J. Ritsema (2000). Seismic evidence for ultralow-velocity zones beneath Africa and eastern Atlantic, *J. Geophys. Res. B Solid Earth Planets* **105,** B10, 23,865–23,878.

Irwan, M., F. Kimata, K. Hirahara, T. Sagiya, and A. Yamagiwa (2004). Measuring ground deformations with 1-Hz GPS data: The 2003 Tokachi-oki earthquake (preliminary report), *Earth Planet Space* **56,** no. 3, 389–393.

Ji, C., K. M. Larson, Y. Tan, K. W. Hudnut, and K. Choi (2004). Slip history of the 2003 San Simeon earthquake constrained by combining 1-Hz GPS, strong motion, and teleseismic data, *Geophys. Res. Lett.* **31,** L17608, doi: 10.1029/2004GL020448.

Kanamori, H. (1993). W Phase, *Geophys. Res. Lett.* **20,** 1691–1694.

Kanamori, H., and L. Rivera (2008). Source inversion of W phase: Speeding up seismic tsunami warning, *Geophys. J. Int.* **175,** no. 1, 222–238, doi: 10.1111/j.1365-246X.2008.03887.x.

Komatitsch, D., and J. Tromp (2002a). Spectral-element simulations of global seismic wave propagation: I. Validation, *Geophys. J. Int.* **149,** 390–412, doi: 10.1046/j.1365-246X.2002.01653.x.

Komatitsch, D., and J. Tromp (2002b). Spectral-element simulations of global seismic wave propagation: II. Three-dimensional models, oceans, rotation and self-gravitation, *Geophys. J. Int.* **150,** 303–318, doi: 10.1046/j.1365-246X.2002.01716.x.

Kouba, J. (2003). Measuring seismic waves induced by large earthquakes with GPS, *Studia Geophysica et Geodaetica* **47,** no. 4, 741–755.

Larson, K. M., A. Bilich, and P. Axelrad (2007). Improving the precision of high-rate GPS, *J. Geophys. Res.* **112,** B05422, doi: 10.1029/2006JB004367.

Larson, K., P. Bodin, and J. Gomberg (2003). Using 1 Hz GPS data to measure deformations caused by the Denali fault earthquake, *Science* **300,** no. 5624, 1421–1424, doi: 10.1126/science.1084531.

Miyazaki, S., T. Iwabuchi, K. Heki, and I. Naito (2003). An impact of estimating tropospheric delay gradients on precise positioning in the summer using the Japanese nationwide GPS array, *J. Geophys. Res.* **108,** no. B7, 2335, doi: 10.1029/2000JB000113.

Ni, S. D., and D. V. Helmberger (2001). Horizontal transition from fast to slow structures at the core-mantle boundary; South Atlantic, *Earth Planet. Sci. Lett.* **187,** nos. 3–4, 301–310.

Ni, S. D., E. Tan, M. Gurnis, and D. V. Helmberger (2002). Sharp sides to the African superplume, *Science* **296,** no. 5574, 1850–1852.

Ohta, Y., I. Meilano, T. Sagiya, F. Kimata, and K. Hirahara (2006). Large surface wave of the 2004 Sumatra-Andaman earthquake captured by the very long baseline kinematic analysis of 1-Hz GPS data, *Earth Planet Space* **58,** no. 2, 153–157.

Shi, C., Y. Lou, H. Zhang, Q. Zhao, J. Geng, R. Wang, R. Fang, and J. Liu (2010). Seismic deformation of the M_w 8.0 Wenchuan earthquake from high-rate GPS observations, *Adv. Space Res.* **46,** no. 2, 228–235, doi: 10.1016/j.asr.2010.03.006.

Simons, M., S. E. Minson, A. Sladen, F. Ortega, J. Jiang, S. E. Owen, L. Meng, J.-P. Ampuero, S. Wei, R. Chu, D. V. Helmberger, H. Kanamori, E. Hetland, A. W. Moore, and F. H. Webb (2011). The 2011 magnitude 9.0 Tohoku-Oki earthquake: Mosaicking the megathrust from seconds to centuries, *Science* **322,** no. 6036, 1421–1425, doi: 10.1126/science.1206731.

Wang, G. Q., D. M. Boore, G. Tang, and X. Zhou (2007). Comparisons of ground motions from co-located and closely spaced one-sample-per-second global positioning system and accelerograph recordings of the 2003 *M* 6.5 San Simeon, California, earthquake in the Parkfield region, *Bull. Seismol. Soc. Am.* **97,** no. 1B, 76–90, doi: 10.1785/0120060053.

Yokota, Y., K. Koketsu, K. Hikima, and S. Miyazaki (2009). Ability of 1-Hz GPS data to infer the source process of a medium-sized earthquake: The case of the 2008 Iwate-Miyagi Nairiku, Japan, earthquake, *Geophys. Res. Lett.* **36,** L12301, doi: 10.1029/2009GL037799.

Yue, H., and T. Lay (2011). Inversion of high-rate (1 sps) GPS data for rupture process of the 11 March 2011 Tohoku earthquake (M_w 9.1), *Geophys. Res. Lett.* **38,** L00G09, doi: 10.1029/2011GL048700.

Zhang, W., and X. Chen (2006). Traction image method for irregular free surface boundaries in finite difference seismic wave simulation, *Geophys. J. Int.* **167,** no. 1, 337–353, doi: 10.1111/j.1365-246X.2006.03113.x.

Zhu, L., and L. A. Rivera (2002). A note on the dynamic and static displacements from a point source in multilayered media, *Geophys. J. Int.* **148,** 619–627, doi: 10.1046/j.1365-246X.2002.01610.x.

Zumberge, J., M. Heflin, D. Jefferson, M. Watkins, and F. Webb (1997). Precise point positioning for the efficient and robust analysis of GPS data from large networks, *J. Geophys. Res.* **102,** 5005–5018.

***Aizhi Guo*[1]**
Yong Wang
Zhiwei Li
Sidao Ni
Genyou Liu
Yong Zheng
State Key Laboratory of Geodesy and Earth's Dynamics
Institute of Geodesy and Geophysics
Chinese Academy of Sciences
Wuhan 430077, China
ywang@whigg.ac.cn

Wenbo Wu
Mengcheng National Geophysical Observatory
School of Earth and Space Sciences
University of Science and Technology of China
Hefei 30026, China

Mark Simons
Seismological Laboratory
California Institute of Technology
Pasadena, California 91125 U.S.A.

[1] Also at Graduate University of Chinese Academy of Sciences, Beijing 100049, China.